European Journal of Radiology 149 (2022) 110194

Contents lists available at ScienceDirect

European Journal of Radiology

journal homepage: www.elsevier.com/locate/ejrad

Research article

Quantification of changes in white matter tract fibers in idiopathic normal pressure hydrocephalus based on diffusion spectrum imaging

Xiaolin Yang [a,b,1], Hongbing Li [c,1], Wenjie He [a,1], Minrui Lv [a], Hong Zhang [a,d], Xi Zhou [a], Haihua Wei [a,b], Boyan Xu [e], Jiakuan Chen [a,f], Haiqin Ma [a,d], Jun Xia [a,*], Guang Yang [g,h]

[a] Department of Radiology, Shenzhen Second People's Hospital/The First Affiliated Hospital of Shenzhen University, Shenzhen 518035, China
[b] The First Clinical Medical College, Guangdong Medical University, Zhanjiang 524023, China
[c] Department of Radiology, Fuyong People's Hospital, Baoan District, Shenzhen 518103, China
[d] Shantou University Medical College, Shantou 515063, China
[e] Beijing Intelligent Brain Cloud Inc, Beijing 100195, China
[f] Guangzhou Medical University, Guangzhou 511436, China
[g] Cardiovascular Research Centre, Royal Brompton Hospital, London SW3 6NP, United Kingdom
[h] National Heart and Lung Institute, Imperial College London, London SW7 2AZ, United Kingdom

ARTICLE INFO

Keywords:
Idiopathic normal pressure hydrocephalus
Diffusion spectrum imaging
White matter
Tract
General fractional anisotropy
Fractional anisotropy

ABSTRACT

Purpose: Patients with idiopathic normal pressure hydrocephalus (iNPH) present white-matter abnormalities. The analytical methods described to date only measure mean diffusion parameter alterations of iNPH-specific brain regions or in a certain fasciculus. This study quantitatively analyzed whether iNPH-tract abnormalities are confined to specific sections or involve entire fibers based on diffusion spectrum imaging (DSI).
Method: Twenty-two patients with iNPH and 20 normally aging subjects were included. The 18 main tracts in the brain of each subject were extracted, and the diffusion parameters of 100 equidistant nodes on each fiber were calculated to quantitatively evaluate integrity changes in different regions along these tracts. Two diffusion metrics were measured, i.e., general fractional anisotropy (GFA) and fractional anisotropy (FA).
Results: Compared to normally aging ($P < 0.05$), in iNPH, the GFA and FA of the left uncinate fasciculus and FA of the bilateral superior longitudinal fasciculus 1 were reduced in areas where the entire fiber was involved (% nodes with significant differences > 90%). Most other fasciculi detected presented GFA or FA alterations limited to specific regions. Increased and decreased GFA or FA co-occurred in different sections of the same fibers, including the corticospinal tract and left thalamic radiation posterior in iNPH.
Conclusions: Few iNPH fibers presented diffusion abnormalities involving nearly all tracts. Most fiber abnormalities in iNPH were confined to specific areas, and different parts of the same fasciculus showed diverse diffusion alterations in few cases. This DSI-based tract analysis provided detailed information on iNPH white-matter changes.

1. Introduction

Idiopathic normal pressure hydrocephalus (iNPH) is a neurological disorder of unknown etiology that can be treated surgically and mainly occurs in elderly individuals [1]. iNPH patients exhibit at least one of the three symptoms of gait disturbance, urinary incontinence, and cognitive impairment [2]. Although lumbar puncture shows cerebrospinal fluid (CSF) pressure within the normal range, iNPH mainly manifests as

Abbreviations: AF, arcuate fasciculus; C, cingulum; C_FP, cingulum frontal parietal; C_FPH, cingulum frontal parahippocampal; C_PH, cingulum parahippocampal; C_PHP, cingulum parahippocampal parietal; C_R, cingulum rarolfactory; CST, corticospinal tract; DSI, diffusion spectrum imaging; DTI, diffusion tensor imaging; FA, fractional anisotropy; GFA, general fractional anisotropy; IFOF, inferior fronto-occipital fasciculus; ILF, inferior longitudinal fasciculus; iNPH, idiopathic normal pressure hydrocephalus; NA, normally aging; SLF, superior longitudinal fasciculus; TR, thalamic radiation; TRA, thalamic radiation anterior; TRP, thalamic radiation posterior; TRS, thalamic radiation superior; UF, uncinate fasciculus.

* Corresponding author.
E-mail address: xiajun@email.szu.edu.cn (J. Xia).

[1] These authors contributed equally to this work and share the first authorship.

https://doi.org/10.1016/j.ejrad.2022.110194
Received 29 November 2021; Received in revised form 20 January 2022; Accepted 29 January 2022
Available online 3 February 2022

ventricle enlargement on radiological images [1,2].

Previous studies have suggested the existence of white-matter abnormalities in iNPH, presumably due to factors such as mechanical pressure caused by ventriculomegaly and metabolic disturbances [3,4]. Although white-matter alterations are observed in iNPH, most previously employed analysis methods could only detect changes in average diffusion tensor imaging (DTI) metrics of brain areas-of-interest (such as the periventricular white matter) or in a specific fiber bundle (such as the corticospinal tract) [4,5].

Whether white-matter fiber abnormalities seen in iNPH are confined to specific tract sections or involve the entire fibers remains unclear. Furthermore, diffusion spectrum imaging (DSI) effectively compensates for the deficiencies of the DTI algorithm and has a higher angular resolution that can precisely show sophisticated cross-winding tracts and fine microstructure white-matter alterations [6,7].

Therefore, this study aimed to use DSI to extract white-matter fibers from the brains of patients with iNPH and to calculate the diffusion parameters of 100 equidistant nodes along each fiber to quantify and evaluate integrity changes in different segments of these tracts. The abnormal regions of the inspected iNPH fibers were located more accurately with a pointwise comparison. We hope that this novel DSI-based tract analysis can identify and more accurately locate abnormal fiber sections, potentially providing new insights into impairment of gait, cognition, and micturition in patients with iNPH.

2. Materials and methods

2.1. Participants

Forty-two dextral subjects participated in this study: 22 patients with iNPH and 20 normally aging (NA) individuals. Based on the iNPH guidelines [1], 22 patients diagnosed with iNPH at our hospital between January 2019 and September 2020 were consecutively included in this study. All 22 patients showed ventricular enlargement as indicated by radiology imaging examinations and at least one of the triad symptoms: gait disorder, cognitive impairment, and urinary incontinence. The study flow chart of the inclusion and exclusion of iNPH and NA participants is shown in Fig. 1. In the early stage of the study, 36 patients with communicating hydrocephalus were registered. Fourteen patients were subsequently excluded because of secondary hydrocephalus (n = 7), no CSF shunting or CSF pressure exceeding the normal threshold (n = 4), magnetic resonance imaging (MRI) contraindications (n = 2), or image artifacts (n = 1).

Related participation advertisements were posted on several billboards of local communities to recruit age-matched healthy aging volunteers (60 to 90 years old) without evident medical histories, such as tumors, cerebrovascular disease, or trauma. Thirty elderly volunteers potentially suitable for the study were recruited. Ten volunteers were excluded following further screening to exclude obvious cerebrovascular diseases (n = 3), white-matter degeneration (n = 1), brain tumor (n = 1), left-handedness (n = 1), MRI contraindications (n = 2), and image artifacts (n = 2). The study was conducted according to the guidelines of the Declaration of Helsinki and approved by our hospital's Ethics Committee. Informed consent was obtained from all participants.

2.2. Magnetic resonance imaging data collection

Patients with iNPH scheduled to undergo MRI examination before surgery were enrolled. All 42 participants were scanned using the same protocol. Using 20-channel phased-array head coils, all subjects completed MRI scans on a 3.0-T MR scanner (Prisma, Siemens, Erlangen, Germany). The MRI scanning session consisted of three-dimensional sagittal T1-weighted magnetization prepared rapid-acquisition gradient echo and DSI sequences. Pulsed gradient twice-refocused spin-echo echo-planar imaging sequences were performed.

The T1-weighted (T1w) acquisition parameters were: repetition time/echo time = 2300/3.55 ms; flip angle, 8°; slice thickness = 0.9 mm; number of sections, 192; field of view (FOV), 240 mm × 240 mm; matrix, 256 × 256; and voxel size = 0.9 mm × 0.9 mm. The DSI collection parameters were: repetition time/echo time = 6300/71 ms;

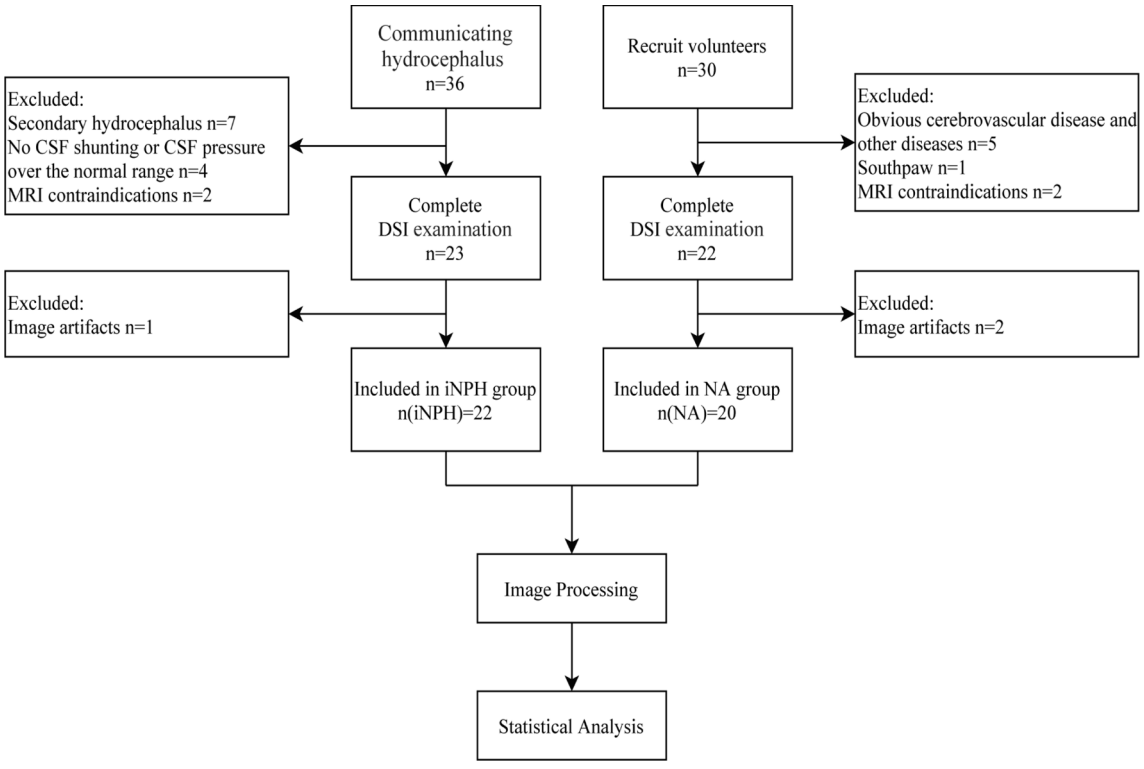

Fig. 1. Study flowchart of the inclusion criteria for iNPH and NA participants. iNPH, idiopathic normal pressure hydrocephalus; NA, normally aging.

slice thickness = 2.2 mm; number of sections on the horizontal axis = 60; FOV = 220 mm × 220 mm; matrix = 100 × 100; and voxel size = 2.2 mm × 2.2 mm × 2.2 mm; total diffusion sampling = 128 and maximum diffusion sensitivity (b-values max) = 3000 s/mm^2. Scan time of DSI was about 15 min.

2.3. Anatomical data preprocessing

Both anatomical and diffusion data were preprocessed using QSIPrep, a robust preprocessing pipeline for diffusion MRI research [8]. The version we used is 0.12.1, which is based on Nipype 1.5.1 [9,10]. The T1w image was corrected for intensity non-uniformity with N4BiasFieldCorrection (ANTs 2.3.1) [11] and used as a T1w reference throughout the workflow. The T1w reference was then skull-stripped using antsBrainExtraction.sh (ANTs 2.3.1) with OASIS as the target template. Spatial normalization to the ICBM 152 nonlinear asymmetrical template version 2009c [12] was performed through nonlinear registration with antsRegistration (ANTs 2.3.1) [13], using the brain-extracted versions of both T1w volume and template. Brain-tissue segmentation of the CSF, white matter, and gray matter was performed on the brain-extracted T1w using FAST (FSL 6.0.3:b862cdd5) [14].

2.4. Diffusion data preprocessing

Initial motion correction was performed only using the b = 0 images. An unbiased b = 0 template was constructed over three iterations of the Affine registrations. The SHORELine method was used to estimate head motion in b > 0 images; this entails excluding each b > 0 image and reconstructing the others using 3dSHORE [15]. The signal for the left image served as the registration target. Two iterations were run using an affine transform. Model-generated images were transformed into an alignment with each b > 0 image. Both slice-wise and whole-brain QC measures (cross-correlation and R^2) were calculated. No susceptibility distortion correction was performed. Several confounding time-series were calculated based on the preprocessed diffusion weighted images (DWI): framewise displacement using the implementation in Nipype, according to the definitions of Power et al. [16]. The head-motion estimates calculated in the correction step were also placed within the corresponding confounds file. The slice-wise cross-correlation was calculated. The DWI time-series were resampled to the anterior commissure-posterior commissure (ACPC), generating a preprocessed DWI run in the ACPC space.

2.5. Tractography and automatic tract recognition

After preprocessing, diffusion data analysis was performed using DSI Studio (http://dsi-studio.labsolver.org), one of the most accurate tractography methods [17]. Augmented fiber tracking was utilized to provide automatic track recognition [18]. Specifically, the diffusion data were reconstructed using generalized q-sampling imaging [19] with a diffusion sampling length ratio of 1.25. A deterministic fiber tracking algorithm [20] was used with augmented tracking strategies [18] to improve reproducibility. Anatomy prior to a tractography atlas [21] was used to map the 18 major fibers (including some subcomponents) with a distance tolerance of 16 mm. Topology-informed pruning [22] was applied to tractography with 32 iterations to remove false connections.

After the tracts were identified, two diffusion parameters were sampled at 100 equidistant points along each tract, including general fractional anisotropy (GFA) and fractional anisotropy (FA). The analyzed tracts included association, commissural, and projection fibers [23], whose directions are respectively regulated as anterior to posterior, right to left, and inferior to superior [24]. These fibers included the corpus callosum forceps minor, corpus callosum forceps major, bilateral arcuate fasciculus (AF), corticospinal tract (CST), cingulum (C), uncinate fasciculus (UF), superior longitudinal fasciculus (SLF), thalamic radiation (TR), inferior longitudinal fasciculus, and inferior fronto-occipital fasciculus. According to the updated HCP1065 atlas [21], three subcomponents of the SLF, SLF 1, 2, and 3, were extracted and analyzed. Similarly, the identified bilateral C was subdivided into the bilateral cingulum frontal parahippocampal, cingulum frontal parietal, cingulum parahippocampal parietal, cingulum parahippocampal, and cingulum rarolfactory; the bilateral TR extracted included the bilateral thalamic radiation anterior (TRA), thalamic radiation posterior (TRP), and thalamic radiation superior (TRS).

2.6. Statistical analysis

T-tests were conducted pointwise along each tract for 100 nodes to compare the diffusion metrics between the iNPH and NA groups. Permutation-based multiple comparison correction was applied to determine statistical significance [25].

3. Results

3.1. Demographics and clinical information

The demographics and clinical information of the iNPH and NA groups are shown in Table 1.

3.2. Fiber tracking and pointwise comparisons along tracts

The successful recognition rates for each of the 18 tracts and their subcomponents in the iNPH and NA groups are detailed in Table 2. The right TRS was successfully tracked in only nine patients with iNPH (the successful recognition rate was only 40.9%). Therefore, we excluded the right TRS from the statistical analysis. A total of 33 fibers were analyzed, including the subcomponents.

The location, number, and percentage of points with significant differences in the pointwise comparisons of GFA and FA across 18 fibers and their subcomponents between the groups are summarized in Table 3. We found that most of the fibers analyzed in patients with iNPH presented abnormal GFA or FA values compared with those in the NA group (family-wise error correction, P < 0.05). Patients with iNPH exhibited abnormal GFA in 70% (23/33) and FA in 67% (22/33) of the examined tracts, and the percentage of nodes with significant differences was 14%–95%.

We also determined that the GFA of the left UF (pointwise changes are shown in Fig. 2) and FA of the left UF and bilateral SLF 1 (Fig. 3) in iNPH decreased in areas where almost the entire fiber was involved (percentage of points with significant differences > 90%). Most of the other tracts analyzed in iNPH had GFA or FA changes relatively confined to specific regions of the fibers (details of pointwise comparison in Figure S1 and Figure S2).

Furthermore, in different components of the same fibers, such as the right CST and left TRP, the GFA was found to both increase and decrease in iNPH (Fig. 4). Increased and decreased FA co-existed in different sections of the bilateral CST and left TRP in iNPH (Fig. 5). Fig. 6 displays GFA maps of a typical iNPH patient and an NA control and the reconstruction results of their left UF, right CST, and left TRP. Most alterations

Table 1
Demographics and clinical information of the iNPH and NA groups.

	iNPH(n = 22)	NA(n = 20)
Age (year)	69.8 ± 7.5	66.5 ± 4.7
Sex (male : female)	13 : 9	11 : 9
Total iNPHGS	4.8 ± 2.5	–
mRS	2.6 ± 0.9	–

Values are expressed as the mean ± standard deviation (SD).
iNPH, idiopathic normal pressure hydrocephalus; NA, normally aging; n, number of total iNPH/NA subjects; iNPHGS, iNPH grading scale; mRS, modified Rankin Scale.

Table 2
Successful recognition rate for each of the 18 tracts and their subcomponents in the iNPH and NA groups.

Number	Tract	n1	n2	Ratio	Ratio
		n(iNPH) = 22	n(NA) = 20	n1/n (iNPH)	n2/n (NA)
1	AF_L	22	20	100.0%	100.0%
2	AF_R	21	20	95.5%	100.0%
3	CST_L	22	20	100.0%	100.0%
4	CST_R	21	20	95.5%	100.0%
5–6	CC				
	Forceps Minor	21	20	95.5%	100.0%
	Forceps Major	17	20	77.3%	100.0%
7–8	Bilateral Cingulum				
	Bilateral C_FPH	22	20	100.0%	100.0%
	Bilateral C_FP	22	20	100.0%	100.0%
	C_PHP_L	20	20	90.9%	100.0%
	C_PHP_R	21	20	95.5%	100.0%
	Bilateral C_PH	22	20	100.0%	100.0%
	Bilateral C_R	22	20	100.0%	100.0%
9–10	Bilateral UF	22	20	100.0%	100.0%
11–12	Bilateral SLF				
	Bilateral SLF 1	19	20	86.4%	100.0%
	SLF 2_L	22	20	100.0%	100.0%
	SLF 2_R	21	20	95.5%	100.0%
	Bilateral SLF 3	22	20	100.0%	100.0%
13–14	Bilateral TR				
	Bilateral TRA	20	20	90.9%	100.0%
	TRP_L	20	20	90.9%	100.0%
	TRP_R	18	20	81.8%	100.0%
	TRS_L	17	19	77.3%	95.0%
	TRS_R	9	20	40.9%	100.0%
15	ILF_L	21	20	95.5%	100.0%
16	ILF_R	22	20	100.0%	100.0%
17	IFOF_L	20	20	90.9%	100.0%
18	IFOF_R	21	20	95.5%	100.0%

iNPH, idiopathic normal pressure hydrocephalus; NA, normally aging; AF, arcuate fasciculus; CST, corticospinal tract; CC, corpus callosum; C_FPH, cingulum frontal parahippocampal; C_FP, cingulum frontal parietal; C_PHP, cingulum parahippocampal parietal; C_PH, cingulum parahippocampal; C_R, cingulum rarolfactory; UF, uncinate fasciculus; SLF, superior longitudinal fasciculus; SLF 1, superior longitudinal fasciculus 1; SLF 2, superior longitudinal fasciculus 2; SLF 3, superior longitudinal fasciculus 3; TR, thalamic radiation; TRA, thalamic radiation anterior; TRP, thalamic radiation posterior; TRS, thalamic radiation superior; ILF, inferior longitudinal fasciculus; IFOF, inferior fronto-occipital fasciculus; L, left; R, right. n1 and n2 represent the successfully recognized number of iNPH and NA subjects in each tract, respectively. n(iNPH), number of total iNPH subjects; n(NA), number of total NA subjects.

in the GFA and FA were similar, but few varied.

4. Discussion

Here, we extracted GFA and FA at 100 equidistant points along the fibers to quantify and assess changes in white-matter integrity across iNPH and NA. Our DSI-based fiber-tract analysis could greatly contribute to iNPH white-matter studies. We found that, in iNPH, most inspected fibers had abnormal GFA or FA properties relative to NA. Furthermore, using a pointwise comparison, this study also revealed position-specific white-matter lesions in iNPH and detailed differences in diffusion alterations along the tracts. In iNPH, few fibers showed diffusion abnormalities involving nearly all tracts. However, most of the tract abnormalities in patients with iNPH were confined to specific areas, and in few cases, different parts of the same fasciculus showed diverse diffusion changes.

Previous studies have mostly relied on DTI to explore white-matter changes in patients with iNPH. Nevertheless, within a unitary voxel, DTI cannot directly image multiple tract orientations [6]. Compared to DTI, DSI has higher angular resolution and can display complex cross-twisted fasciculi [6,7]. Therefore, we opted for DSI to analyze white-matter changes in patients with iNPH. Similar to FA in DTI studies, GFA as a DSI parameter estimates the integrity changes of white matter, varying from 0 (indicating entirely isotropic diffusion) to 1 (indicating diffusion that is obviously limited to one dimension) [26]. Although GFA has been reported to correlate with FA, both parameters are to varying degrees dependent on the partial volume of the crossing fibers and the crossing angle [27]. As for the tracts analyzed here, the statistical results regarding GFA and FA were relatively consistent, but some regions of a few fibers displayed dissimilarly. We hypothesized that DSI differed from DTI in processing cross-fibers, which might lead to small deviations in the analysis results. A further study should be conducted.

Many studies have revealed that white-matter abnormalities in patients with iNPH are prominent [2]. Our study found that most of the fasciculi examined in iNPH had abnormal GFA or FA values, suggesting that patients with iNPH present widespread changes in the white-matter integrity of the brain. This wide range of detected diffusion changes in patients with iNPH is consistent with previous findings of studies using different analytical methods such as tract-based spatial statistics and multiple regions of interest [4,5]. Previous iNPH studies have demonstrated mean diffusion parameter alterations in brain regions-of-interest or in a certain tract. Whether the abnormalities of these fibers in iNPH are confined to specific areas of the tracts or involve the entire fibers remains unclear. This question cannot be accurately answered based on average diffusion parameter analysis, which is incapable of showing the positioning characteristics of white-matter integrity changes along each fiber.

Thus, it is necessary to use a quantitative analysis method of pointwise comparison to locate the abnormal fiber section and determine the specific white-matter abnormality pattern within it, which will provide more detailed information regarding white-matter integrity changes in patients with iNPH. Using a pointwise comparison, this study revealed that the GFA and FA of the left UF and FA of the bilateral SLF 1 in iNPH were reduced in areas where almost the entire fasciculus was involved (percentage of points with significant differences $>$ 90%). A great portion of the other tracts analyzed had GFA or FA changes that were relatively limited to some specific regions of the fibers. Thus, by extracting fibers and quantifying diffusion metric alterations point-by-point, any abnormal sections or details of the inspected fibers in iNPH can be more accurately detected, which cannot be achieved with the same precision using an average diffusion parameter analysis.

Some studies have reported reduced FA in the subcortical or periventricular white matter in patients with hydrocephalus [4]. The decrease in FA value is mostly attributed to the mechanical pressure caused by the expansion of the ventricle stretching and compressing the structures of periventricular white matter and corpus callosum, resulting in loss of fiber integrity and axon lesions [4,28]. However, some studies have shown increased FA in fiber systems next to the ventricles, including the CST in patients with hydrocephalus [4,5]. The enlargement of the ventricle mechanically stretched and compressed the axons of the nerve fibers, causing water molecules to be arranged in the same direction of the axons, indicating increased FA [4,5]. FA values of some sensorimotor-related thalamic nuclei in early-stage iNPH patients were raised, which were considered to be possibly related to the improvement of nerve conduction efficiency and sensorimotor neuroplasticity [29]. Additionally, FA values lower at specific locations where the tracts cross, and the reduction in cross-fiber integrity may lead to increased FA [30]. FA values were found to increase and decrease in different brain regions of iNPH, and these changes were partially reversible after shunting [31]. Another study found no significant differences in GFA and FA of the CST between patients with iNPH and healthy controls [32]. These phenomena appear contradictory.

Our study showed that a large part of the fasciculi detected in iNPH had decreased GFA or FA across a portion or almost the entire tract. Some sections of a few fibers in iNPH showed an increase in GFA or FA, such as the right AF and TRA, left TRS, and bilateral CST and TRP. Notably, variable changes in diffusion in different regions of the same

Table 3
Location, number, and percentage of points with significant differences in pointwise comparisons of the GFA and FA across the 18 fibers and their subcomponents between the iNPH and NA groups.

Number	Tract	GFA			FA		
		Location of points*	Number of points	Percentage of points	Location of points*	Number of points	Percentage of points
1	AF_L	73-87↓	15↓	15%↓	69-88↓	20↓	20%↓
2	AF_R	34-52↑	19↑	19%↑	0	0	0
3	CST_L	48-75↑	28↑	28%↑	53-72↑, 78-96↓	20↑, 19↓	20%↑, 19%↓
4	CST_R	26-41↑, 51-75↑, 81-94↓	41↑, 14↓	41%↑, 14%↓	55-72↑, 77-96↓	18↑, 20↓	18%↑, 20%↓
5–6	CC						
	Forceps Minor	18-93↓	76↓	76%↓	6-93↓	88↓	88%↓
	Forceps Major	6-26↓, 37-50↓, 74-96↓	58↓	58%↓	5-28↓, 33-65↓, 72-96↓	82↓	82%↓
7–8	Bilateral Cingulum						
	Bilateral C_FPH	0	0	0	0	0	0
	Bilateral C_FP	0	0	0	0	0	0
	Bilateral C_PHP	0	0	0	0	0	0
	C_PH_L	11-79↓	69↓	69%↓	9-98↓	90↓	90%↓
	C_PH_R	6-65↓	60↓	60%↓	5-83↓	79↓	79%↓
	Bilateral C_R	0	0	0	0	0	0
9	UF_L	7-100↓	94↓	94%↓	6-100↓	95↓	95%↓
10	UF_R	0	0	0	0	0	0
11–12	Bilateral SLF						
	SLF 1_L	3-91↓	89↓	89%↓	1-91↓	91↓	91%↓
	SLF 1_R	3-30↓, 42-93↓	80↓	80%↓	2-94↓	93↓	93%↓
	SLF 2_L	5-32↓, 64-93↓	58↓	58%↓	5-35↓, 61-94↓	65↓	65%↓
	SLF 2_R	6-34↓	29↓	29%↓	5-38↓, 71-91↓	55↓	55%↓
	SLF 3_L	5-47↓, 49-93↓	88↓	88%↓	6-93↓	88↓	88%↓
	SLF 3_R	12-32↓, 70-86↓	38↓	38%↓	13-33↓, 68-86↓	40↓	40%↓
13–14	Bilateral TR						
	TRA_L	0	0	0	23-39↓	17↓	17%↓
	TRA_R	82-95↑	14↑	14%↑	0	0	0
	TRP_L	23-61↑, 66-85↓	39↑,20↓	39%↑, 20%↓	25-40↑, 65-84↓	16↑, 20↓	16%↑, 20%↓
	TRP_R	25-41↑	17↑	17%↑	67-82↓	16↓	16%↓
	TRS_L	5-59↑	55↑	55%↑	65-88↓	24↓	24%↓
	TRS_R	–	–	–	–	–	–
15	ILF_L	22-96↓	75↓	75%↓	11-96↓	86↓	86%↓
16	ILF_R	67-93↓	27↓	27%↓	67-94↓	28↓	28%↓
17	IFOF_L	60-95↓	36↓	36%↓	11-26↓, 61-94↓	50↓	50%↓
18	IFOF_R	73-86↓	14↓	14%↓	8-24↓, 73-92↓	37↓	37%↓

iNPH, idiopathic normal pressure hydrocephalus; NA, normally aging; AF, arcuate fasciculus; CST, corticospinal tract; CC, corpus callosum; C_FPH, cingulum frontal parahippocampal; C_FP, cingulum frontal parietal; C_PHP, cingulum parahippocampal parietal; C_PH, cingulum parahippocampal; C_R, cingulum rarolfactory; UF, uncinate fasciculus; SLF, superior longitudinal fasciculus; SLF 1, superior longitudinal fasciculus 1; SLF 2, superior longitudinal fasciculus 2; SLF 3, superior longitudinal fasciculus 3; TR, thalamic radiation; TRA, thalamic radiation anterior; TRP, thalamic radiation posterior; TRS, thalamic radiation superior; ILF, inferior longitudinal fasciculus; IFOF, inferior fronto-occipital fasciculus; L, left; R, right; GFA, general fractional anisotropy; FA, fractional anisotropy. *, association, commissural, and projection fibers, whose directions are respectively regulated as anterior to posterior, right to left, and inferior to superior; ↓, GFA/FA value decreased; ↑, GFA/FA value increased; 0, no significant difference between the groups; -, no statistical analysis.

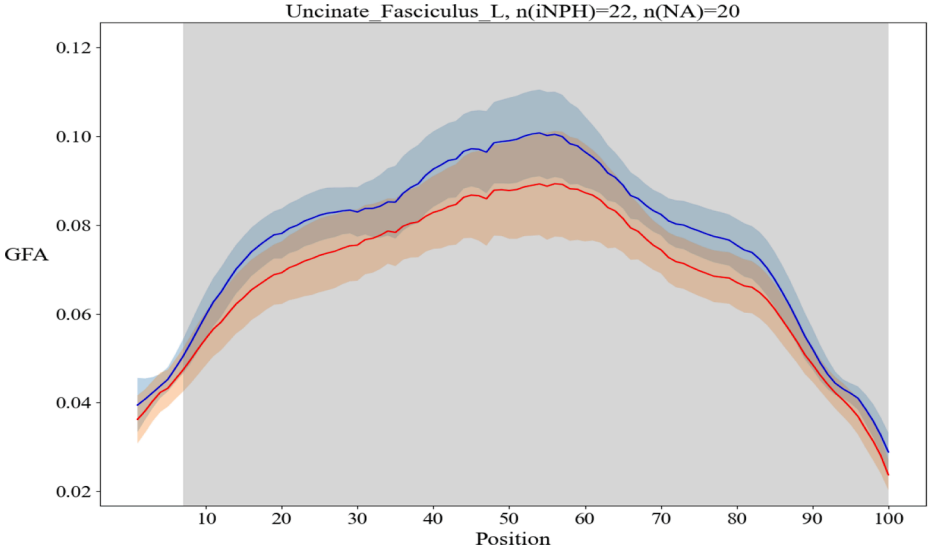

Fig. 2. Pointwise comparison of the GFA of the left uncinate fasciculus (UF) between the groups (percentage of points with significant differences > 90%). The shaded areas indicate the confidence interval, and the gray-shaded parts are the positions with significant differences in the analyzed fiber variables between the iNPH (red) and NA (blue) groups (family-wise error correction, $P < 0.05$). iNPH, idiopathic normal pressure hydrocephalus; NA, normally aging; L, left; GFA, general fractional anisotropy; n (iNPH), successfully recognized number of patients with iNPH in the left UF; n (NA), successfully recognized number of NA subjects in the left UF.

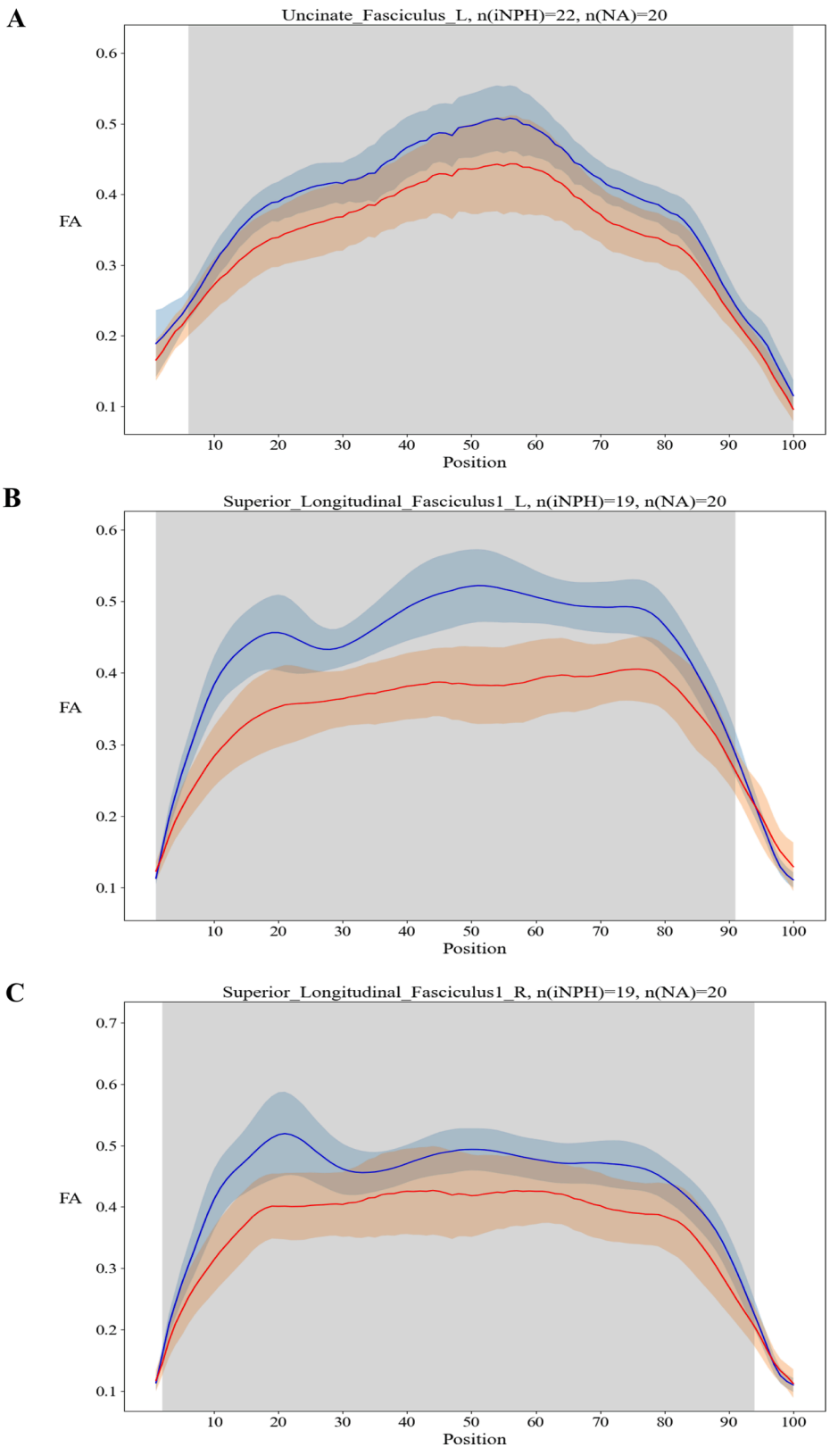

Fig. 3. Pointwise changes in the FA of the left uncinate fasciculus (UF) and bilateral superior longitudinal fasciculus 1 (SLF 1) between the groups (percentage of points with significant differences > 90%). The shaded areas indicate the confidence interval, and the gray shaded parts are the positions of significant differences in the variables of the analyzed fibers between the iNPH (red) and NA (blue) groups (family-wise error correction, $P < 0.05$). (A) Pointwise comparison of the FA of the left UF between the groups. (B-C) Pointwise comparison of the FA of the bilateral SLF 1 between the groups. iNPH, idiopathic normal pressure hydrocephalus; NA, normally aging; L, left; R, right; FA, fractional anisotropy; n (iNPH), successfully recognized number of patients with iNPH in the corresponding tract; n (NA), successfully recognized number of NA subjects in the corresponding tract.

fasciculus in iNPH also occurred. For example, in patients with iNPH, the FA increased significantly in the middle and superior segments of the bilateral CST and decreased significantly at the top section. No FA abnormalities were observed in the inferior portion of the bilateral CST. These changes in the FA of the CST shown here were similar to those reported by previous studies [4]. In addition to the CST, GFA and FA were also seen to both increase and decrease in different portions of the left TRP. Therefore, we believe that these phenomena are reasonable and not contradictory. We suggest that these differences may be due to the co-existence of higher or lower GFA or FA in different sections of

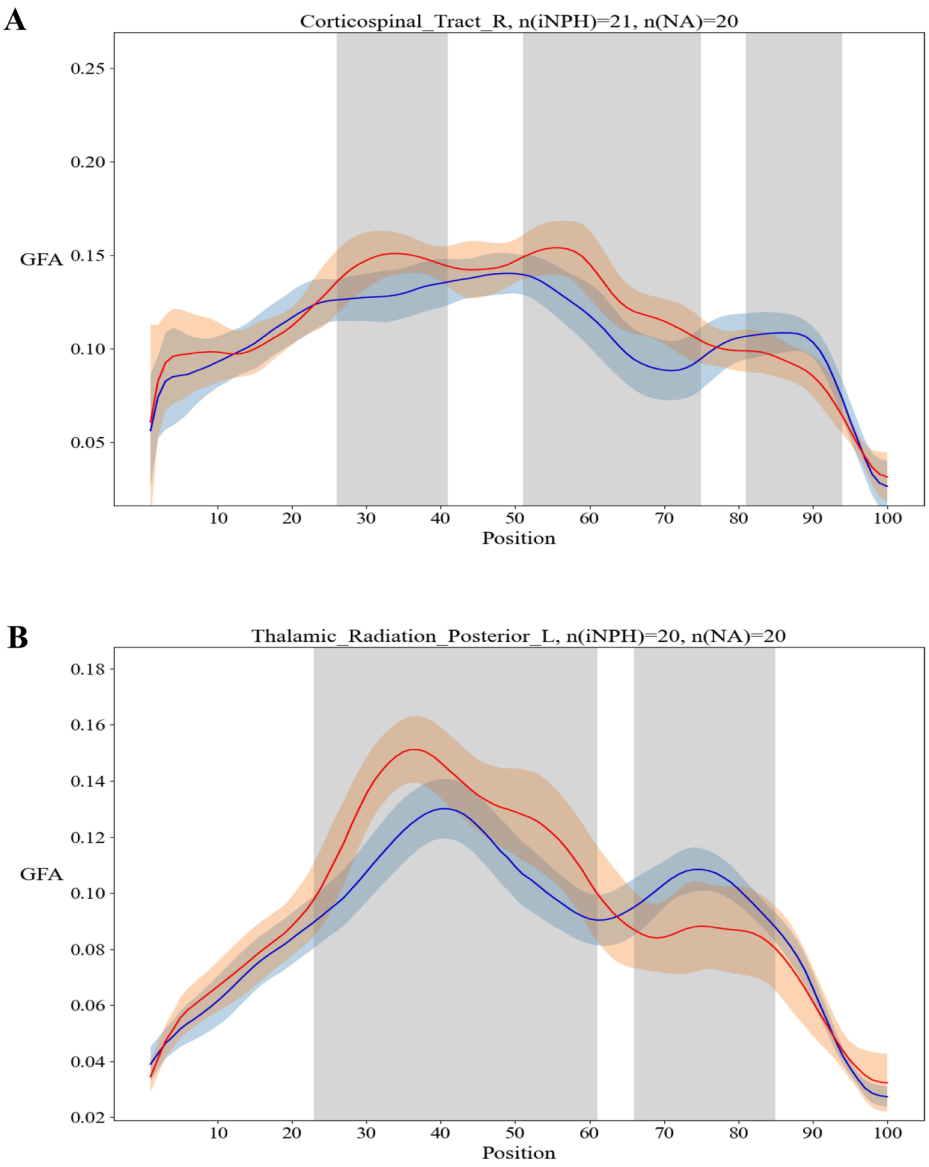

Fig. 4. Increased and decreased GFA appear to co-occur in different sections of the right corticospinal tract (CST) and left thalamic radiation posterior (TRP). The shaded areas indicate the confidence interval, and the gray shaded parts are the positions of significant difference in the analyzed fibers between the iNPH (red) and NA (blue) groups (family-wise error correction, $P < 0.05$). (A) Pointwise comparison of the GFA of the right CST between the groups. (B) Pointwise comparison of the GFA of the left TRP between the groups. iNPH, idiopathic normal pressure hydrocephalus; NA, normally aging; L, left; R, right; GFA, general fractional anisotropy; n (iNPH), successfully recognized number of patients with iNPH in the corresponding tract; n (NA), successfully recognized number of NA subjects in the corresponding tract.

white-matter fibers, or the two may offset each other [32], whereby only a change in the average value of GFA or FA was often detected. Through point-by-point comparative analysis, we found that the white-matter integrity changes in iNPH were comprehensive processes, and these phenomena may co-occur.

There were some limitations to this study. First, the ventricles of patients with iNPH were greatly enlarged, which might have a technical impact on the results of fiber tracking and abnormalities in the observed tract analysis. Although the preprocessing and analysis tools have been validated [8,17], the additional error induced by enlarged ventricles should be further elucidated. In particular, low tract identification rates may be partially due to this issue. Here, the right TRS failed to be extracted from several patients with iNPH. It should be noted that strict criterion was commonly used in automatic fiber identification to remove false tracts and ensure the correctness of the identified fibers, which is another reason for the failed identification of fibers [33]. Augmented fiber tracking should be further tuned to increase the accuracy for iNPH patients. Second, all patients were recruited at a single center. This is a rudimentary study, and future studies are expected to investigate the clinical relevance of changes in these diffusion parameters across tracts in iNPH.

5. Conclusion

This study found that iNPH caused widespread changes in the white-matter integrity of the brain. Our study used a point-by-point comparison to reveal that, in iNPH, few tracts demonstrated diffusion abnormalities involving nearly all fibers. Nevertheless, most of the fasciculus abnormalities in iNPH were relatively confined to specific areas, and in few cases, different sections of the same fasciculus showed varying diffusion alterations. This study, along with tract analysis based on DSI, provided additional details regarding changes in the white matter of patients with iNPH.

Institutional Review Board Statement

The study was conducted according to the guidelines of the Declaration of Helsinki and approved by the Ethics Committee of The First Affiliated Hospital of Shenzhen University and Shenzhen Second People's hospital.

Informed Consent Statement

Informed consent was obtained from all the participants.

Data Availability Statement

The data presented in this study are available on request from the corresponding author.

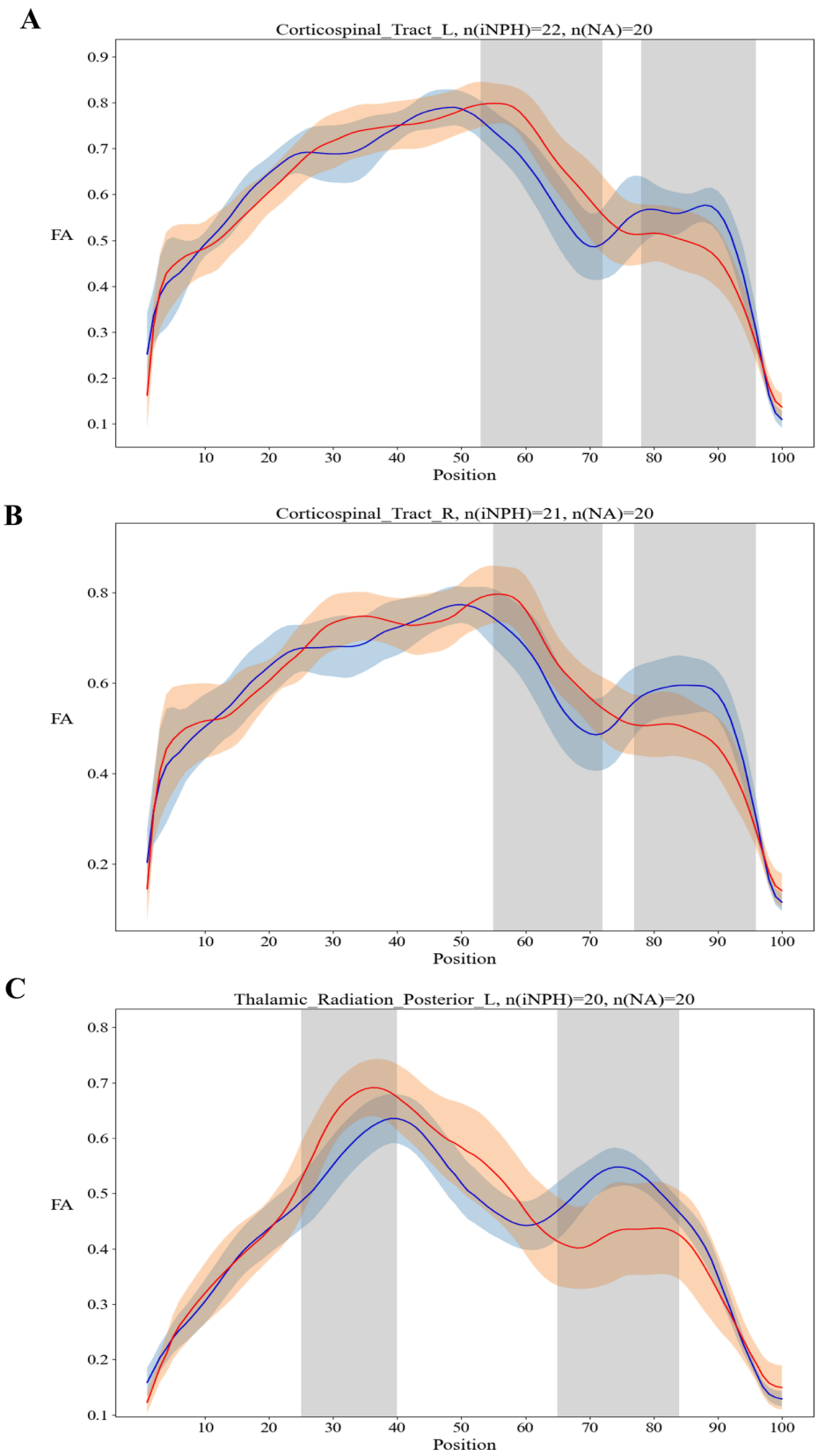

Fig. 5. Increased and decreased FA appear together in different portions of the bilateral corticospinal tract (CST) and left thalamic radiation posterior (TRP). The shaded areas indicate the confidence interval, and the gray shaded parts are the positions with significant differences in the analyzed fibers between the iNPH (red) and NA (blue) groups (family-wise error correction, $P < 0.05$). (A-B) Pointwise changes in the FA of the bilateral CST between the groups. (C) Pointwise changes in the FA of the left TRP between the groups. iNPH, idiopathic normal pressure hydrocephalus; NA, normally aging; L, left; R, right; FA, fractional anisotropy; n (iNPH), successfully recognized number of patients with iNPH in the corresponding tract; n (NA), successfully recognized number of NA subjects in the corresponding tract.

CRediT authorship contribution statement

Xiaolin Yang: Conceptualization, Methodology, Investigation, Data curation, Formal analysis, Visualization, Writing – original draft. **Hongbing Li:** Conceptualization, Investigation, Writing – original draft. **Wenjie He:** Conceptualization, Methodology, Validation, Data curation, Writing – original draft. **Minrui Lv:** Methodology, Investigation, Formal analysis. **Hong Zhang:** Investigation, Data curation. **Xi Zhou:**

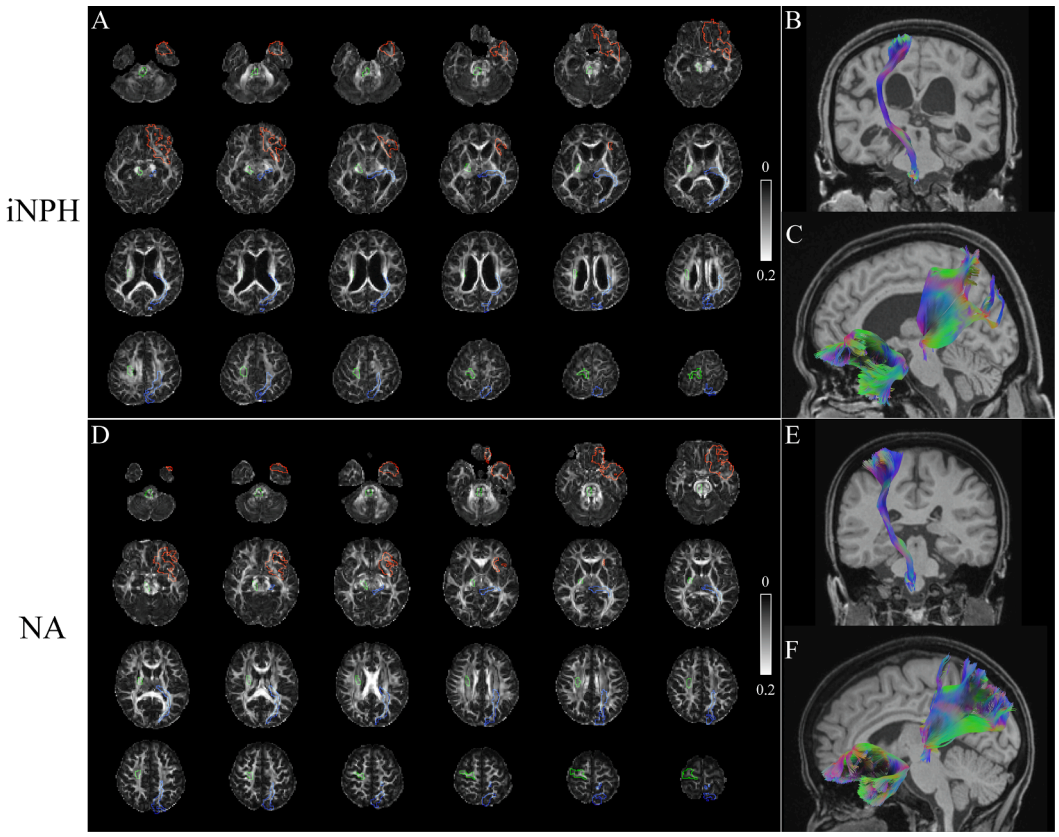

Fig. 6. GFA maps of a typical iNPH patient and an NA control and the reconstruction results of their left UF, right CST, and left TRP. (A and D) GFA maps of iNPH and NA. Colorbar from 0 (black) to 0.2 (white). Red, green, and blue respectively indicate the range of the left UF, right CST, and left TRP. (B and E) The reconstruction results of the right CST. (C and F) The reconstruction results of the left UF and left TRP. GFA, general fractional anisotropy; iNPH, idiopathic normal pressure hydrocephalus; NA, normally aging; UF, uncinate fasciculus; CST, corticospinal tract; TRP, thalamic radiation posterior.

Investigation. **Haihua Wei:** Investigation. **Boyan Xu:** Software, Validation, Visualization. **Jiakuan Chen:** Investigation. **Haiqin Ma:** Investigation. **Jun Xia:** Validation, Resources, Data curation, Supervision, Funding acquisition, Project administration, Writing – review & editing. **Guang Yang:** Validation, Supervision, Writing – review & editing.

Declaration of Competing Interest

The authors declare the following financial interests/personal relationships which may be considered as potential competing interests: [Boyan Xu is employed by Beijing Intelligent Brain Cloud Inc., Beijing, China. The remaining authors declare that the research was conducted in the absence of any commercial or financial relationships that could be construed as a potential conflict of interest].

Acknowledgments

We would like to thank the patients and volunteers who participated in this study and all researchers who assisted in data collection and management.

Funding

This work was supported in part by the National Natural Science Foundation of China [grant number 82171913]; the Natural Science Foundation of Guangdong Province [grant number 2020A1515010918]; the Project of Shenzhen Basic Development Project [grant number JCYJ20190806164409040]; the MRC [grant number MC/PC/21013]; and the UKRI Future Leaders Fellowship [grant number MR/V023799/1].

Appendix A. Supplementary material

Supplementary data to this article can be found online at https://doi.org/10.1016/j.ejrad.2022.110194.

References

[1] M. Nakajima, S. Yamada, M. Miyajima, K. Ishii, N. Kuriyama, H. Kazui, H. Kanemoto, T. Suehiro, K. Yoshiyama, M. Kameda, Y. Kajimoto, M. Mase, H. Murai, D. Kita, T. Kimura, N. Samejima, T. Tokuda, M. Kaijima, C. Akiba, K. Kawamura, M. Atsuchi, Y. Hirata, M. Matsumae, M. Sasaki, F. Yamashita, S. Aoki, R. Irie, H. Miyake, T. Kato, E. Mori, M. Ishikawa, I. Date, H. Arai, Guidelines for management of idiopathic normal pressure hydrocephalus (Third Edition): Endorsed by the Japanese society of normal pressure hydrocephalus, Neurol. Med. Chir. (Tokyo) 61 (2) (2021) 63–97, https://doi.org/10.2176/nmc.st.2020-0292.

[2] Z. Wang, Y. Zhang, F. Hu, J. Ding, X. Wang, Pathogenesis and pathophysiology of idiopathic normal pressure hydrocephalus, CNS. Neurosci. Ther. 26 (12) (2020) 1230–1240, https://doi.org/10.1111/cns.13526.

[3] M.R. Del Bigio, M.J. Wilson, T. Enno, Chronic hydrocephalus in rats and humans: white matter loss and behavior changes, Ann. Neurol. 53 (3) (2003) 337–346, https://doi.org/10.1002/ana.10453.

[4] T. Hattori, K. Ito, S. Aoki, T. Yuasa, R. Sato, M. Ishikawa, H. Sawaura, M. Hori, H. Mizusawa, White matter alteration in idiopathic normal pressure hydrocephalus: tract-based spatial statistics study, AJNR, Am. J. Neuroradiol. 33 (1) (2012) 97–103, https://doi.org/10.3174/ajnr.A2706.

[5] E. Hattingen, A. Jurcoane, J. Melber, S. Blasel, F.E. Zanella, T. Neumann-Haefelin, O.C. Singer, Diffusion tensor imaging in patients with adult chronic idiopathic hydrocephalus, Neurosurgery. 66 (2010) 917–924, https://doi.org/10.1227/01.NEU.0000367801.35654.EC.

[6] V.J. Wedeen, R.P. Wang, J.D. Schmahmann, T. Benner, W.Y.I. Tseng, G. Dai, D. N. Pandya, P. Hagmann, H. D'Arceuil, A.J. de Crespigny, Diffusion spectrum magnetic resonance imaging (DSI) tractography of crossing fibers, Neuroimage. 41 (4) (2008) 1267–1277, https://doi.org/10.1016/j.neuroimage.2008.03.036.

[7] B. Leng, S. Han, Y. Bao, H. Zhang, Y. Wang, Y. Wu, Y. Wang, The uncinate fasciculus as observed using diffusion spectrum imaging in the human brain, Neuroradiology. 58 (6) (2016) 595–606, https://doi.org/10.1007/s00234-016-1650-9.

[8] M. Cieslak, P.A. Cook, X. He, F.-C. Yeh, T. Dhollander, A. Adebimpe, G.K. Aguirre, D.S. Bassett, R.F. Betzel, J. Bourque, L.M. Cabral, C. Davatzikos, J.A. Detre, E. Earl, M.A. Elliott, S. Fadnavis, D.A. Fair, W. Foran, P. Fotiadis, E. Garyfallidis, B. Giesbrecht, R.C. Gur, R.E. Gur, M.B. Kelz, A. Keshavan, B.S. Larsen, B. Luna, A. P. Mackey, M.P. Milham, D.J. Oathes, A. Perrone, A.R. Pines, D.R. Roalf, A. Richie-Halford, A. Rokem, V.J. Sydnor, T.M. Tapera, U.A. Tooley, J.M. Vettel, J. D. Yeatman, S.T. Grafton, T.D. Satterthwaite, QSIPrep: an integrative platform for preprocessing and reconstructing diffusion MRI data, Nat Methods 18 (7) (2021) 775–778, https://doi.org/10.1038/s41592-021-01185-5.

[9] K. Gorgolewski, C.D. Burns, C. Madison, D. Clark, Y.O. Halchenko, M.L. Waskom, S. S. Ghosh, Nipype: a flexible, lightweight and extensible neuroimaging data processing framework in python, Front. Neuroinform. 5 (2011) 13, https://doi.org/10.3389/fninf.2011.00013.

[10] K.J. Gorgolewski, T. Nichols, D.N. Kennedy, J.B. Poline, R.A. Poldrack, Making replication prestigious, Behav. Brain. Sci. 41 (2018), e131, https://doi.org/10.1017/S0140525X18000663.

[11] N.J. Tustison, B.B. Avants, P.A. Cook, Y. Zheng, A. Egan, P.A. Yushkevich, J.C. Gee, N4ITK: improved N3 bias correction, IEEE. Trans. Med, Imaging. 29 (2010) 1310–1320, https://doi.org/10.1109/TMI.2010.2046908.

[12] U. Yoon, V.S. Fonov, D. Perusse, A.C. Evans, W.S. Ball, A.W. Byars, M. Schapiro, W. Bommer, A. Carr, A. German, S. Dunn, M.J. Rivkin, D. Waber, R. Mulkern, S. Vajapeyam, A. Chiverton, P. Davis, J. Koo, J. Marmor, C. Mrakotsky, R. Robertson, G. McAnulty, M.E. Brandt, J.M. Fletcher, L.A. Kramer, G. Yang, C. McCormack, K.M. Hebert, H. Volero, K. Botteron, R.C. McKinstry, W. Warren, T. Nishino, C.R. Almli, R. Todd, J. Constantino, J.T. McCracken, J. Levitt, J. Alger, J. O'Neil, A. Toga, R. Asarnow, D. Fadale, L. Heinichen, C. Ireland, D.J. Wang, E. Moss, R.A. Zimmerman, B. Bintliff, R. Bradford, J. Newman, A.C. Evans, R. Arnaoutelis, G.B. Pike, D.L. Collins, G. Leonard, T. Paus, A. Zijdenbos, S. Das, V. Fonov, L. Fu, J. Harlap, I. Leppert, D. Milovan, D. Vins, T. Zeffiro, J. Van Meter, N. Lange, M.P. Froimowitz, K. Botteron, C.R. Almli, C. Rainey, S. Henderson, T. Nishino, W. Warren, J.L. Edwards, D. Dubois, K. Smith, T. Singer, A.A. Wilber, C. Pierpaoli, P.J. Basser, L.C. Chang, C.G. Koay, L. Walker, L. Freund, J. Rumsey, L. Baskir, L. Stanford, K. Sirocco, K. Gwinn-Hardy, G. Spinella, J.T. McCracken, J. R. Alger, J. Levitt, J. O'Neill, The effect of template choice on morphometric analysis of pediatric brain data, Neuroimage. 45 (2009) 769–777, https://doi.org/10.1016/j.neuroimage.2008.12.046.

[13] B. Avants, C. Epstein, M. Grossman, J. Gee, Symmetric diffeomorphic image registration with cross-correlation: evaluating automated labeling of elderly and neurodegenerative brain, Med. Image. Anal. 12 (1) (2008) 26–41, https://doi.org/10.1016/j.media.2007.06.004.

[14] Y. Zhang, M. Brady, S. Smith, Segmentation of brain MR images through a hidden Markov random field model and the expectation-maximization algorithm, IEEE. Trans. Med, Imaging. 20 (2001) 45–57, https://doi.org/10.1109/42.906424.

[15] S.L. Merlet, R. Deriche, Continuous diffusion signal, EAP and ODF estimation via Compressive Sensing in diffusion MRI, Med. Image. Anal. 17 (5) (2013) 556–572, https://doi.org/10.1016/j.media.2013.02.010.

[16] J.D. Power, A. Mitra, T.O. Laumann, A.Z. Snyder, B.L. Schlaggar, S.E. Petersen, Methods to detect, characterize, and remove motion artifact in resting state fMRI, Neuroimage. 84 (2014) 320–341, https://doi.org/10.1016/j.neuroimage.2013.08.048.

[17] K.H. Maier-Hein, P.F. Neher, J.-C. Houde, M.-A. Côté, E. Garyfallidis, J. Zhong, M. Chamberland, F.-C. Yeh, Y.-C. Lin, Q. Ji, W.E. Reddick, J.O. Glass, D.Q. Chen, Y. Feng, C. Gao, Y.e. Wu, J. Ma, R. He, Q. Li, C.-F. Westin, S. Deslauriers-Gauthier, J.O.O. González, M. Paquette, S. St-Jean, G. Girard, F. Rheault, J. Sidhu, C.M. W. Tax, F. Guo, H.Y. Mesri, S. Dávid, M. Froeling, A.M. Heemskerk, A. Leemans, A. Boré, B. Pinsard, C. Bedetti, M. Desrosiers, S. Brambati, J. Doyon, A. Sarica, R. Vasta, A. Cerasa, A. Quattrone, J. Yeatman, A.R. Khan, W. Hodges, S. Alexander, D. Romascano, M. Barakovic, A. Auría, O. Esteban, A. Lemkaddem, J.-P. Thiran, H. E. Cetingul, B.L. Odry, B. Mailhe, M.S. Nadar, F. Pizzagalli, G. Prasad, J.E. Villalon-Reina, J. Galvis, P.M. Thompson, F.D.S. Requejo, P.L. Laguna, L.M. Lacerda, R. Barrett, F. Dell'Acqua, M. Catani, L. Petit, E. Caruyer, A. Daducci, T.B. Dyrby, T. Holland-Letz, C.C. Hilgetag, B. Stieltjes, M. Descoteaux, The challenge of mapping the human connectome based on diffusion tractography, Nat Commun 8 (1) (2017), https://doi.org/10.1038/s41467-017-01285-x.

[18] F.-C. Yeh, Shape analysis of the human association pathways, Neuroimage. 223 (2020) 117329, https://doi.org/10.1016/j.neuroimage.2020.117329.

[19] F.C. Yeh, V.J. Wedeen, W.Y. Tseng, Generalized q-sampling imaging, IEEE. Trans. Med Imaging. 29 (2010) 1626–1635, https://doi.org/10.1109/TMI.2010.2045126.

[20] F.C. Yeh, T.D. Verstynen, Y. Wang, J.C. Fernández-Miranda, W.Y. Tseng, Deterministic diffusion fiber tracking improved by quantitative anisotropy, PLoS One. 8 (2013) e80713. https://doi.org/10.1371/journal.pone.0080713.

[21] F.C. Yeh, S. Panesar, D. Fernandes, A. Meola, M. Yoshino, J.C. Fernandez-Miranda, J.M. Vettel, T. Verstynen, Population-averaged atlas of the macroscale human structural connectome and its network topology, Neuroimage. 178 (2018) 57–68, https://doi.org/10.1016/j.neuroimage.2018.05.027.

[22] F.-C. Yeh, S. Panesar, J. Barrios, D. Fernandes, K. Abhinav, A. Meola, J. C. Fernandez-Miranda, Automatic removal of false connections in diffusion MRI tractography using topology-informed pruning (TIP), Neurotherapeutics. 16 (1) (2019) 52–58, https://doi.org/10.1007/s13311-018-0663-y.

[23] J.D. Yeatman, R.F. Dougherty, N.J. Myall, B.A. Wandell, H.M. Feldman, Tract profiles of white matter properties: automating fiber-tract quantification, PLoS One. 7 (2012) e49790. https://doi.org/10.1371/journal.pone.0049790.

[24] Y.-J. Chen, Y.-C. Lo, Y.-C. Hsu, C.-C. Fan, T.-J. Hwang, C.-M. Liu, Y.-L. Chien, M. H. Hsieh, C.-C. Liu, H.-G. Hwu, W.-Y. Tseng, Automatic whole brain tract-based analysis using predefined tracts in a diffusion spectrum imaging template and an accurate registration strategy, Hum. Brain. Mapp. 36 (9) (2015) 3441–3458, https://doi.org/10.1002/hbm.22854.

[25] T.E. Nichols, A.P. Holmes, Nonparametric permutation tests for functional neuroimaging: a primer with examples, Hum. Brain. Mapp. 15 (1) (2002) 1–25, https://doi.org/10.1002/hbm.1058.

[26] T.-H. Tsai, H.-T. Su, Y.-C. Hsu, Y.-C. Shih, C.-C. Chen, F.-R. Hu, W.-Y. Tseng, White matter microstructural alterations in amblyopic adults revealed by diffusion spectrum imaging with systematic tract-based automatic analysis, Br. J. Ophthalmol. 103 (4) (2019) 511–516, https://doi.org/10.1136/bjophthalmol-2017-311733.

[27] K.H. Fritzsche, F.B. Laun, H.-P. Meinzer, B. Stieltjes, Opportunities and pitfalls in the quantification of fiber integrity: what can we gain from Q-ball imaging? Neuroimage 51 (1) (2010) 242–251, https://doi.org/10.1016/j.neuroimage.2010.02.007.

[28] Y. Ding, J.P. McAllister, B. Yao, N. Yan, A.I. Canady, Axonal damage associated with enlargement of ventricles during hydrocephalus: a silver impregnation study, Neurol. Res. 23 (6) (2001) 581–587, https://doi.org/10.1179/016164101101199045.

[29] P.-H. Tsai, Y.-C. Chen, S.-W. Chiang, T.-Y. Huang, M.-C. Chou, H.-S. Liu, H.-W. Chung, G.-S. Peng, H.-I. Ma, H.-W. Kao, C.-Y. Chen, Changes in sensorimotor-related thalamic diffusion properties and cerebrospinal fluid hydrodynamics predict gait responses to tap test in idiopathic normal-pressure hydrocephalus, Eur. Radiol. 28 (11) (2018) 4504–4513, https://doi.org/10.1007/s00330-018-5488-x.

[30] Y. Masutani, S. Aoki, O. Abe, N. Hayashi, K. Otomo, MR diffusion tensor imaging: recent advance and new techniques for diffusion tensor visualization, Eur. J. Radiol. 46 (1) (2003) 53–66.

[31] A. Eleftheriou, I. Blystad, A. Tisell, J. Gasslander, sF. Lundin, Publisher Correction: Indication of Thalamo-Cortical Circuit Dysfunction in Idiopathic Normal Pressure Hydrocephalus: A Tensor Imaging Study. Sci Rep 10(2020). 12014. https://doi.org/10.1038/s41598-020-63238-7.

[32] H. Zhang, W.J. He, L.H. Liang, H.W. Zhang, X.J. Zhang, L. Zeng, S.P. Luo, F. Lin, Y. Lei, Diffusion spectrum imaging of corticospinal tracts in idiopathic normal pressure hydrocephalus, Front. Neurol. 12 (2021), 636518, https://doi.org/10.3389/fneur.2021.636518.

[33] H. Chen, X. Sheng, R. Qin, C. Luo, M. Li, R. Liu, B. Zhang, Y. Xu, H. Zhao, F. Bai, Aberrant White Matter Microstructure as a Potential Diagnostic Marker in Alzheimer's Disease by Automated Fiber Quantification, Front Neurosci 14(570123 (2020), https://doi.org/10.3389/fnins.2020.570123.